Aircraft-based mass balance estimate of methane emissions from offshore gas facilities in the Southern North Sea

Magdalena Pühl[1], Anke Roiger[1], Alina Fiehn[1], Alan M. Gorchov Negron[2], Eric A. Kort[2], Stefan Schwietzke[3], Ignacio Pisso[4], Amy Foulds[5], James Lee[6], James L. France[3,7,8], Anna E. Jones[7], Dave Lowry[8], Rebecca E. Fisher[8], Langwen Huang[5], Jacob Shaw[5,a], Prudence Bateson[5], Stephen Andrews[6], Stuart Young[6], Pamela Dominutti[9], Tom Lachlan-Cope[7], Alexandra Weiss[7], Grant Allen[5]

[1]Deutsches Zentrum für Luft- und Raumfahrt (DLR), Institut für Physik der Atmosphäre, Oberpfaffenhofen, Germany
[2] Department of Climate and Space Sciences and Engineering, University of Michigan, Ann Arbor, MI, USA
[3] Environmental Defense Fund, Berlin, Germany
[4] Norwegian Institute for Air Research (NILU), Kjeller, Norway
[5] Department of Earth and Environmental Science, University of Manchester, Manchester, M13 9PL, UK
[6] National Centre for Atmospheric Science, University of York, York, YO10 5DQ, UK
[7] British Antarctic Survey, Natural Environment Research Council, Cambridge CB3 0ET, UK
[8] Department of Earth Sciences, Royal Holloway, University of London, Egham TW20 0EX, UK
[9] Université Grenoble Alpes, UMR 5001, CNRS, IRD, Grenoble, 38000, France
[a] now at: National Physical Laboratory (NPL), Hampton Road, Teddington, TW11 0LW, UK

Correspondence to: M. Pühl (Magdalena.puehl@dlr.de)

Abstract. Atmospheric methane (CH_4) concentrations have more than doubled since the beginning of the industrial age, making CH_4 the second most important anthropogenic greenhouse gas after carbon dioxide (CO_2). The oil and gas sector represent one of the major anthropogenic CH_4 emitters as it is estimated to account for 22% of global anthropogenic CH_4 emissions. An airborne field campaign was conducted in April-May 2019 to study CH_4 emissions from offshore gas facilities in the Southern North Sea with the aim to derive emission estimates using a top-down (measurement-led) approach. We present CH_4 fluxes for six UK and five Dutch offshore platforms/platform complexes using the well-established mass balance flux method. We identify specific gas production emissions and emission processes (venting/fugitive or flaring/combustion) using observations of co-emitted ethane (C_2H_6) and CO_2. We compare our top-down estimated fluxes with a ship-based top-down study in the Dutch sector and with bottom-up estimates from a globally gridded annual inventory, UK national annual point-source inventories, and with operator-based reporting for individual Dutch facilities. In this study, we find that all inventories, except for the operator-based facility-level reporting, underestimate measured emissions, with the largest discrepancy observed with the globally gridded inventory. Individual facility reporting, as available for Dutch sites for the specific survey date, shows better agreement with our measurement-based estimates. For all sampled Dutch installations together, we find that our estimated flux of (122.9 ± 36.8) kg h^{-1} deviates by a factor 0.64 (0.33-12) from reported values (192.8 kg h^{-1}). Comparisons with aircraft observations in two other offshore regions (Norwegian Sea and Gulf of Mexico) show that measured, absolute facility-level emission rates agree with the general distribution found in other offshore basins despite different production types

(oil, gas) and gas production rates, which vary by two orders of magnitude. Therefore, mitigation is warranted equally across
35   geographies.

1 Introduction

Atmospheric CH_4 mole fractions have more than doubled since 1750 due to human activity and continue to rise (Saunois et al., 2020). According to the NOAA Global Monitoring Laboratory, globally-averaged atmospheric CH_4 is estimated to have experienced the most dramatic annual increase in 2021 since the beginning of the measurements in 1984 (Lan et al., 2022).
40   With a factor 80-83 times stronger global warming potential over a 20-year time horizon compared to CO_2, CH_4 is the second-most important anthropogenic greenhouse gas after CO_2 and contributes 16% to the effective radiative forcing of well-mixed greenhouse gases over 1750-2019 (Forster et al., 2021). Considering its short life time of around a decade, CH_4 bears a high potential for mitigation strategies in order to reach the aim of the UNFCCC Paris Agreement to abate climate warming (Nisbet et al., 2019). Recently, the European Union and the UK signed up to the Global Methane Pledge with the aim to cut global
45   CH_4 emissions by at least 30% from 2020 levels by 2030 (European Commission, United States of America, 2021).

The oil and gas sector has been estimated to account for 22 (18-27)% of global anthropogenic CH_4 emissions (bottom-up 2017; Saunois et al., 2020). Onboard offshore oil and gas platforms, CH_4 is emitted during routine operations due to safety and operational reasons (e.g. shutdown or start-up of equipment during production) by either controlled venting or flaring, i.e., the release of gas or burning of gas. In the latter case, CO_2 is released simultaneously, with the CH_4/CO_2 emission ratio dependent
50   on the flaring efficiency. According to the United Kingdom Continental Shelf (UKCS) Flaring & Venting report (Oil and Gas Authoritgy (OGA), 2020), in 2019 a total of 2600 metric tonnes (t) CH_4 was emitted in the Southern North Sea and the minor Irish Sea region, of which 74% comes from venting, 13% from turbines and engines, 10% are fugitive emissions (e.g. from leaky valves or compressors) and 3% flaring. Carbon dioxide emission was 0.8 Mt in the same year, arising mainly from turbines and engines (95%) with minor contribution of flaring (4%) and venting (0.01%). Flaring accounts for 87% and venting
55   13% of the total CO_2 and CH_4 emissions from venting and flaring. Flaring emissions consist of 99% CO_2 and 1% CH_4 and venting emissions of 98% CH_4 and 2% CO_2. Dutch CH_4 emissions from the extraction of crude oil and natural gas on the Netherlands Continental Shelf (Dutch Pollutant Release and Transfer Register, 2019) amount to 6500 t in 2019, of which 98% comes from venting and fugitives, 1.6% from the usage of natural gas (e.g. as fuel for combustion) and 0.2% from flaring. Carbon dioxide emission was 1.1 Mt with a share of 99% from usage of natural gas, 0.8% from flaring and 0.2% from venting
60   and fugitives. Flaring accounts for 33% and venting/fugitives 67% of the total CO_2 and CH_4 emissions from venting/fugitives and flaring. Flaring emissions consist of 99.7% CO_2 and 0.3% CH_4 and venting/fugitive emissions are 89% CH_4 and 11% CO_2.

In Europe the UK is the second largest and the Netherlands the third largest natural gas producer after Norway (Eurostat, 2018). Most of the UK offshore dry gas production takes place in the Southern North Sea region, which comprises 81 dry gas

fields with 181 installations. In 2019, 492 bcf (billion cubic feet) of dry gas was produced. In comparison, the Dutch offshore gas production was 348 bcf from 181 offshore gas fields located in the Southern North Sea.

Several studies indicate that bottom-up inventories underestimate emissions from the oil and gas industry (MacKay et al., 2021; Saunois et al., 2020; Gorchov Negron et al., 2020; Schwietzke et al., 2016; Pétron et al., 2012). Unintended leaks can significantly contribute to CH_4 emissions (Varon et al., 2019; Pandey et al., 2019; Lee et al., 2018; Zavala-Araiza et al., 2017; Conley et al., 2016; Lyon et al., 2015). Top-down emission estimates from direct measurements close to sources can help to independently validate bottom-up estimates in inventory data. A better understanding, monitoring and verification of CH_4 emissions associated with oil/gas operations is crucial part of the European Methane strategy (European Commission, 2020).

Studies on measurements of CH_4 emissions from offshore platforms are still rare. Ship-based measurements were conducted in the U.S. Gulf of Mexico (Yacovitch et al., 2020), in Southeast Asia (Nara et al., 2014) and in the North Sea (Riddick et al., 2019; Hensen et al., 2019). CH_4 emissions from the vicinity of 3 UK gas platforms in the Southern North Sea measured by Riddick et al., 2018, are 17.6 - 20.5 kg h^{-1}. In this study, observations were taken onboard small boats at an altitude of ~2.5 m (above sea level). The measurements relied on a Gaussian plume model to estimate the vertical resolution of a plume, resulting in a total uncertainty of 45%. Hensen et al., 2019, determined CH_4 fluxes around 5 Dutch facilities in the Southern North Sea using a combination of measurements taken 35 m above sea level, a Gaussian plume model and a tracer-release experiment. The results range from 10 kg h^{-1} to 194 kg h^{-1}.

In contrast to ship-based measurements, the mobility of aircraft allows for sampling of emission plumes both horizontally and vertically, and thus, airborne measurements provide more detailed information on marine boundary layer conditions which are known to be complex. To the best of our knowledge, the only airborne measurements around offshore facilities conducted so far took place in the Sureste Basin, Mexico (Zavala-Araiza et al., 2021), in the U.S. Gulf of Mexico (Gorchov Negron et al., 2020), in the Norwegian Sea (Foulds et al., 2022; Roiger et al., 2015) and in the North Sea (Lee et al., 2018; Cain et al., 2017). Lee et al., 2018, determined CH_4 fluxes higher than 4500 kg h^{-1} arising from an uncontrolled CH_4 blow out around one installation in the Central North Sea.

Our paper is organized as follows: In Section 2, we briefly introduce the aircraft instrumentation and sampling strategy applied during the field campaign in the Southern North Sea. We describe the mass balance method used for the calculation of CH_4 fluxes and give an overview of the emission inventories. In Section 3, we discuss our measurements and compare the estimated fluxes with the annualized Global Fuel Exploitation Inventory (GFEI) (Scarpelli et al., 2019), UK annually reported data (UK National Atmospheric Emissions Inventory (NAEI), UK Environmental and Emissions Monitoring System database (EEMS)), and with individual reporting by operators of the sampled Dutch platforms. Additionally, we compare our estimated fluxes with ship-based measurements, which were taken around the sampled Dutch platforms in 2018 (Hensen et al., 2019). Finally, we set the findings into a wider context by comparing them with results from aircraft observations in two other offshore regions (Norwegian Sea (Foulds et al., 2022), Gulf of Mexico (Gorchov Negron et al., 2020)).

2 Materials and Methods

2.1 Campaign 2018/2019 in the Southern North Sea

In April-May 2019 airborne measurements of emissions from offshore installations in the Southern North Sea were conducted within the framework of the United Nations Climate & Clean Air Coalition (UN CCAC) objective to help characterize global CH_4 emissions arising from the oil and gas industry. In a previously conducted campaign in 2018, regional survey flights were performed for method development purposes. In 2019, the flight strategy was adapted in order to sample emissions from dedicated installations, which were chosen because of available inventory emission estimates (UK sites, NAEI) and previous ship-borne measurements (NL sites, Hensen et al., 2019). France et al. (2021) describe the instrument payload and the sampling strategy for both campaigns. Here we extend this study with a quantification of CH_4 emissions for the studied offshore platforms in 2019.

Figure 1 depicts the flight patterns for 2019. A total of five flights were conducted in the Southern North Sea region. Both UK and Dutch sites of offshore gas facilities were surveyed. One flight (F326) was aborted due to poor weather conditions. Platform positions were taken from the Oil and Gas Authority (OGA) for UK sites and the Dutch Oil and gas portal (NLOG) for Dutch sites. Multiple vertically stacked transects in a 2D plane were flown downwind of targeted platforms to fully capture the vertical extent of a plume. Measurements were made at distances varying from 2 to 7 km from the facilities at altitudes between 45 m - 1300 m above sea level. The flights took place in the afternoon hours, when the boundary layer was expected to be well-mixed. The boundary layer height was determined from abrupt changes in observed potential temperature gradient which mark the boundary layer top, using meteorological data sampled during the vertical profiling of the aircraft.

The DHC6 Twin Otter research aircraft, operated by the British Antarctic Survey (BAS), was equipped with several instruments to collect in situ data of atmospheric trace gases. A Picarro G2311-f 10 Hz Analyser measured dry-air CH_4 and CO_2 mole fractions at a response time of 0.4 s and at a precision of 1.2 ppb (1σ @ 1 Hz) for CH_4. A tuneable infrared laser direct absorption spectrometer (TILDAS, Aerodyne Research Inc.) was deployed to detect C_2H_6 (response time < 2 s; precision 50 ppt over 10 s) (Yacovitch et al., 2014). To assess boundary layer physics, sensors for temperature, pressure, humidity and 3D-wind were mounted at the front nose of the aircraft. A NOAA "Best Air Turbulence" probe was installed at the boom of the aircraft and provided wind measurements at a resolution of 50 Hz (Weiss et al., 2011; Garman et al., 2006). More details on the instrumentation and its calibration procedures are given in France, et. al. (2021).
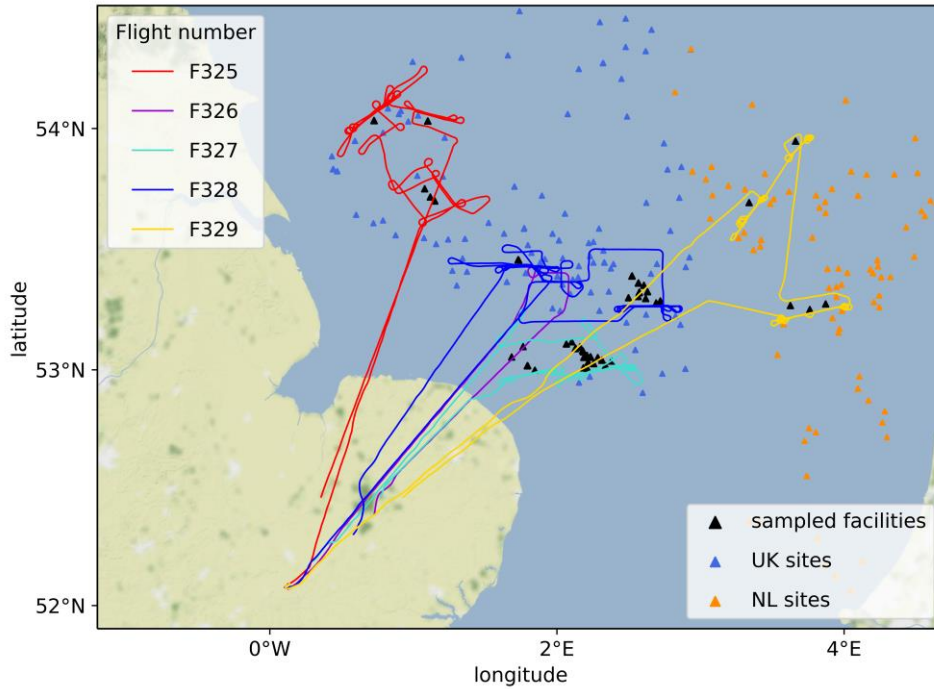
Figure 1. Aircraft tracks for the 2019 campaign in the Southern North Sea (lines). Location of all offshore facilities in the UK (blue markers) and Dutch (orange markers) region and the sampled facilities (black markers).

2.2 Flux calculation method

We apply the mass balance method to determine the amount of CH_4 emitted by the platforms/ multi-platform complexes and
125   passing through a 2D vertical plane downwind (e.g. Pitt et al., 2019; Klausner et al., 2018; O'Shea et al., 2014). For the flux calculation, measured wind speeds in the target region are required to be relatively steady. In general, the mass balance method is applied with the approximation that the plume is vertically well-mixed within the planetary boundary layer. However, to reduce the uncertainty of this approximation under the given meteorological conditions, we conduct horizontal transects at several altitudes to get a higher resolution of the dispersed plume in the vertical. Thereby, we subdivide the 2D vertical plane
130   into discrete mixing layers to account for a possible non-uniformly spread plume. Equation (1) is used to derive the CH_4 flux (unit mass per time) across each individual horizontal transect i within the plane, followed by an integration over the vertical plume extent:

$$Flux_i \ = \Delta C_i \cdot \frac{p_i \cdot M}{R \cdot T_i} \cdot V_\perp \cdot \ \Delta x_i \cdot D_i \tag{1}$$

ΔC_i represents the difference of CH_4 mole fractions measured in- (C_i) and outside (C_0) of the plume ($\Delta C_i = C_i - C_0$). The
135   background mole fractions C_0 during the time of flight through the plume are individually calculated for each transect. Thereby we use the average CH_4 mole fractions over a 30 s time span at either side of the plume and interpolate linearly in between to

account for any drift in background. CH$_4$ mole fractions are converted to a CH$_4$ mass density by applying the ideal gas law, i.e. multiplication with molar mass M, the ideal gas constant R and measured pressure p_i and temperature T_i. The CH$_4$ mass density is then multiplied with the average wind speed $V_\perp$ perpendicular to the flight track, which is calculated from the measured average wind speed, wind direction and aircraft heading over all transects. Finally, the CH$_4$ flux for each single transect is obtained by multiplying with the plume width Δx_i and the vertical depth of each mixing layer D_i. The enhancement measured in each transect is assumed for a layer reaching halfway to the next upper/lower transect. We use all horizontal transects for the flux calculation with the highest transect, where enhancements are found, as the upper plume boundary. In the case where CH$_4$ enhancements were detected up to the highest transect of the aircraft, we use the boundary layer height as the maximal upper plume boundary assuming that the entrainment flux is small. The boundary layer height is inferred from inspection of the vertical gradient of the potential temperature, which is calculated using the in-situ measured meteorological parameters (Stull, 1988). In case of enhanced CH$_4$ being detected in the lowest transect, the surface is assumed as lower plume boundary.

As a result, the bulk net CH$_4$ flux through the plane $Flux_{total}$ is the sum over the fluxes $Flux_i$ calculated for each transect i where CH$_4$ was enhanced:

$$Flux_{total} = \sum_{i}^{transects} Flux_i \tag{2}$$

Our flux calculation method is similar to the method applied by Foulds et al. (2022), but differs slightly in the calculation of ΔC_i. Foulds et al. (2022) calculate the background CH$_4$ mole fractions over a greater time period (50 s) due to a more variable CH$_4$ background seen in the Norwegian Continental Shelf. In the Appendix A, the CH$_4$ flux calculation is illustrated by using observations of platform P1 on 30 April 2019. Detailed information on the uncertainty calculation method is provided in the Appendix B.

2.3 Emission inventories

In our comparison with bottom-up estimates we refer to a globally gridded annual inventory based on IPCC Tier 1 methods (IPCC, 2006), UK national point-source inventories and facility-level reporting by Dutch operators.

2.3.1 Globally gridded annual inventory of CH$_4$ emissions from fossil fuels exploitation

The Global Fuel Exploitation Inventory (GFEI) (Scarpelli et al., 2019) is a globally gridded 0.1° x 0.1° inventory containing CH$_4$ emissions arising from fossil fuel exploitation for the year 2019. National emission totals, which are based on country-specific emission factors, are reported to the UNFCCC (United Nations Framework Convention on Climate Change) and used in the inventory for a spatial downscaling to the locations of potential sources (Scarpelli, 2020). Thereby, global data sets for oil and gas infrastructure are used. The UK UNFCCC reporting for emissions from the offshore oil and gas exploitation is based on the UK Environmental and Emissions Monitoring System (EEMS) database (Brown et al., 2022) and the Dutch reporting is based on the Dutch Pollutant Release and Transfer Register (Honig et al., 2022). In the UNFCCC reported data,

fugitive emissions are already categorized into subsectors, whereas venting and flaring emissions are reported as totals. Thus, the latter are disaggregated by the inventory to the subsectors using IPCC Tier 1 methods (IPCC, 2006). As a result, the inventory resolves the different fossil fuels sectors (oil, gas, coal) and associated subsectors (distribution (fugitive), exploration (fugitive + venting + flaring), processing (fugitive, flaring), production (fugitive, flaring), storage (fugitive) and transmission (fugitive, venting)). We compare our emission estimates with the GFEI v2 data set for total global fuel exploitation for gas from the Harvard Dataverse (Scarpelli et al., 2019). Thereby, we take the inventory data given for each grid cell (Mt/km^2) and calculate the emission from the grid cell area.

2.3.2 UK annual point-source inventories

The UK Environmental and Emissions Monitoring System (EEMS) database is the environmental database of the UK oil and gas industry maintained by the Offshore Petroleum Regulator for Environment and Decommissioning (OPRED) and the UK Department for Business, Energy & Industrial Strategy (BEIS). It provides annual data from measurements and calculations made for single offshore installations based on reported data from operators. According to the EEMS Atmospheric Emission Calculations (OPRED (BEIS), 2008), monitoring systems of emitted gases are rare at offshore installations. Where no direct measurement data is available, the emission is calculated by the inventory multiplying activity data (e.g. fuel consumption or flow to flare/venting stack) with locally derived or default emission factors, which are mainly taken from literature. Inventory sources for CH_4 and CO_2 are differentiated into: engines, heaters and turbines for either diesel, fuel oil or gas consumption; total fugitive emissions; gas flaring from maintenance, routine or upsets/other; total gas venting and emissions from ship oil loading. Latest EEMS data is available for 2018 and 2019.

The UK National Atmospheric Emissions Inventory (NAEI) is an emission database listing all UK point-sources and is provided by BEIS. For offshore oil and gas installations it is based on the Emissions Trading Scheme (ETS) dataset for combustion and flaring sources and on the EEMS inventory for fugitives, venting and other sources such as oil loading (with combustion and flaring data only used if not available in ETS) (Brown et al., 2023; personal communication with the technical director for the NAEI). The inventory compilation process includes quality checks against other reporting systems such as the Petroleum Production Reporting System (PPRS), which also reports venting, flaring and gas use data. In the NAEI inventory, emission data is aggregated for all platforms associated with a certain oil or gas field (NAEI, 2020). Offshore emission data is available for CH_4 and for CO_2. The fluxes observed in this study arise from installations within a certain field and are compared to the inventory data from 2018.

2.3.3 Facility-level reporting by platform operators for the survey date

For the sampled Dutch sites facility-level operator-based reporting on CH_4 emission was provided after the flights. The OGMP 2.0 level of the reporting corresponds to level 3, i.e. using generic emission factors for individual source types. The reporting comprises information on the status of the installation (producing or offline on an hourly basis), the total amount of gas

produced and CH_4 and CO_2 emissions on the survey day including additional information on emission types and sources (venting, flaring, fugitives). Such information was unavailable for the UK facilities upon request via the trade association Oil & Gas UK.

3 Results

The flight conditions during the flights selected for this study were generally good with moderate wind speeds (3-8 m/s). The number of horizontal transects conducted downwind of the sampled installations and used for the flux calculation range from 4 to 9. For one flight the flux calculation for two installations was not successful due to a poorly defined plume. As a result, CH_4 emission fluxes have been determined for six UK and five Dutch facilities sampled during flight surveys on 30 April 2019, 2 May 2019 and 6 May 2019, using the mass balance method described above. The installations, for which the flux calculation was successful, comprise 17% of the UK SNS dry gas production (OGA, 2019) and 6% of the Dutch offshore dry gas production (NLOG, 2019). Under the prevailing conditions found during the three flights, the level of detection, which is a result of the maximum uncertainty of all measured flux calculation parameters (wind speed $V_\perp$, layer depth D_i, CH_4 enhancement ΔC_i, pressure p_i, temperature T_i, plume width Δx_i), is 0.3 kg h^{-1} (2σ). No CH_4 enhancement was detected downstream of 4 out of 11 specifically targeted platforms (P3, P5, P6, P9 in Table 1). In addition, a number of several other platforms were passed downwind with no indication of CH_4 enhancements. These observations are listed in the Appendix E.

In this section we compare our measured CH_4 fluxes with reported emissions and ship-based measurements for Dutch sites. Further, we present observed correlations between CH_4, C_2H_6 and CO_2.

3.1 Comparison of calculated and reported CH4 fluxes

In the following, the top-down results of the 2019 measurements are compared to the most recent available bottom-up estimates from globally gridded and national point-source annual inventories from the years 2018 (NAEI, EEMS), 2019 (EEMS, GFEI) and to daily operator-based facility-level reporting. We also compare our results to a ship-based top-down study conducted by Hensen et al., 2019, for the sampled Dutch sites. Observational based top-down methods only provide "snap-shot" emission estimates representing emissions only for the time of the measurements. This means that a) to allow for a comparison the yearly inventory data needs to be scaled to the temporal resolution of the measurement (or vice-versa), and b) a detailed one-by-one comparison is hampered, which is especially true for cases when observations are made during times of non-typical operational conditions, as well as for intermittent emissions (Foulds et al., 2022; Chen et al., 2022). Therefore, for the comparison with inventories a set of "snap-shot" measurements around a group of sites, which represent a distribution of emissions in a region, are preferred over a one-by-one comparison (Tullos et al., 2021).

Figure 2 and Table 1 show the estimated top-down CH_4 fluxes along with the reported bottom-up fluxes for all sampled installations P1-P11. Typically, one installation denotes a platform for drilling, accommodation and production. P3 consists of

3 platforms, and P6 has one central platform with 3 satellite platforms. P4 and P5, both multi-platform complexes, have two central platforms with a compression unit and a terminal and several more producing platforms around. P4 consists of two central platforms, 6 platforms for production and 3 wellhead platforms (19 platforms in total). P5 has two central platforms, 4 platforms for production and 3 wellhead platforms (15 platforms in total). Emissions in both regions are the same magnitude and range from 12.1 kg h^{-1} to 86.5 kg h^{-1}. Only the multi-platform complex P4 stands out with higher emissions (1258.7 kg h^{-1}). The relative uncertainties of the determined fluxes range from 23% to 70% with the wind measurements as main contributor (> 90%).
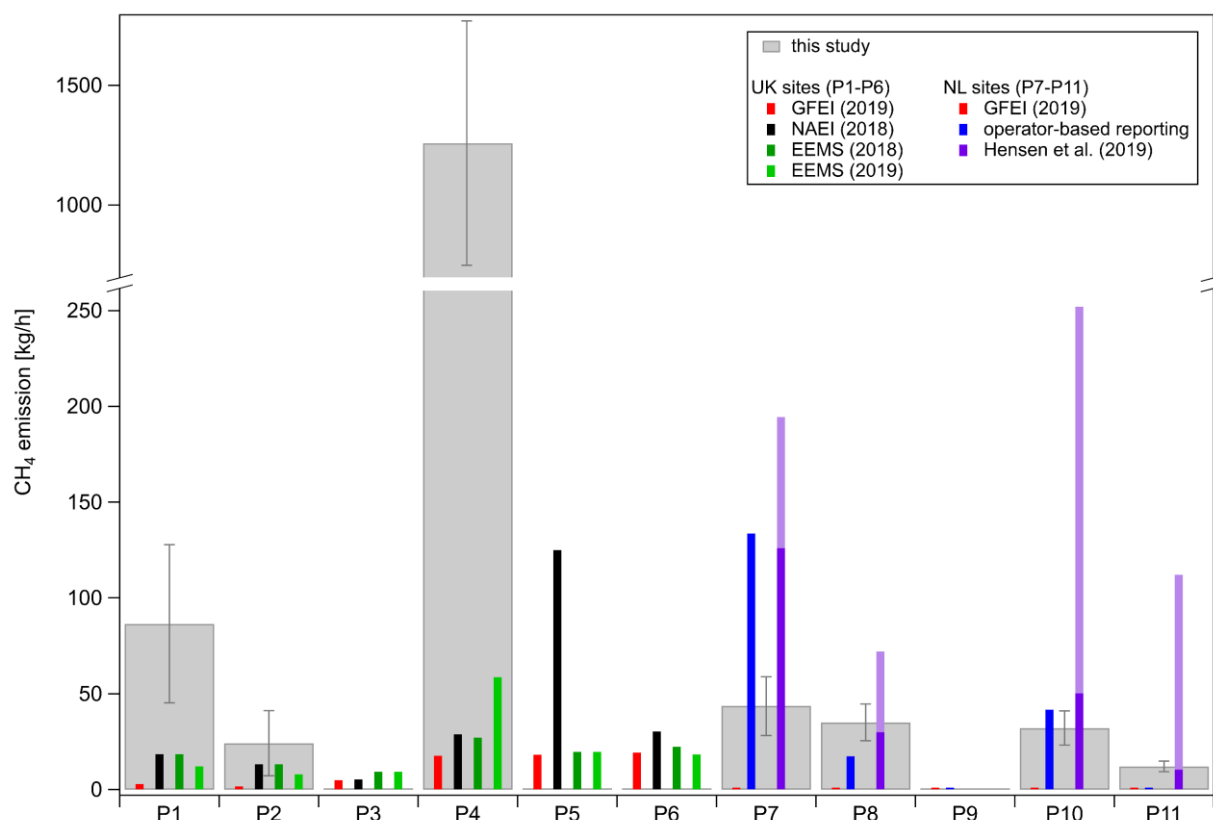
Figure 2. Comparison of calculated CH$_4$ fluxes from this study (grey) for UK sites (P1-P6) and Dutch sites (P7-P11) to the Global Fuel Exploitation Inventory (GFEI; red), the UK National Atmospheric Emissions Inventory (NAEI; black), UK Environmental and Emissions Monitoring System database (EEMS; dark green for 2018; light green for 2019), reported fluxes from operators (blue) and a ship-based top-down study (range in light purple; minimal flux in dark purple) for Dutch sites (Hensen et al., 2019). The inventory annual emission data is converted to hourly emissions. For 4 out of 11 targeted installations no downwind enhancements were detected (P3, P5, P6, P9). GFEI (2019) emission data for P7-P11 and operator-based reporting for P9 and P11 is smaller than 0.3 kg h^{-1}. Operator reported values were not available for UK sites.

Table 1. Observed CH4 fluxes for UK and Dutch sites from this study and emissions from annual reporting from the UK National Atmospheric Emissions Inventory (NAEI, 2018), the UK Environmental and Emissions Monitoring System database (EEMS, 2018 and 2019) and the Global Fuel Exploitation Inventory (GFEI, 2019). For 4 out of the 11 targeted installations emissions are measured to be below the level of detection (LoD, 0.3 kg h⁻¹). Data from individual operator-based reporting on the specific survey date was available only for Dutch sites. Information on emission processes is given for venting (vent), fugitives (fug) and flaring (flar). Results from a ship-based top-down study (Hensen et al., 2019) is listed for 4 out of 5 sampled Dutch sites.

Survey date		30 April 2019	2 May 2019				6 May 2019				
Country		UK		UK				NL			
Installation		P1	P2	P3	P4 complex	P5 complex	P6	P7	P8	P9	P10	P11
CH4 flux [kg h⁻¹] This study	all	86.5 ± 41.2	24.2 ± 17.0	<LoD	1258.7 ± 510.1	<LoD	<LoD	43.6 ± 15.4	35.1 ± 9.6	<LoD	32.1 ± 9.0	12.1 ± 2.8
GFEI (2019)	all	2.9	1.6	4.9	18.1	19.3	19.1	0.21	0.21	0.003	0.006	0.01
	gas processing - fug	1.3	0	0	0	0	7.5	0	0	0	0	0
	gas processing - flar	1.2	0	0	0	0	7.3	0.2	0.2	0	0	0
	gas production - flar	0.1	0.5	1.4	5.2	5.6	1.3	0.005	0.006	0.003	0.006	0.01
	gas exploration - fug, vent, flar	0.3	1.1	3.5	12.9	13.7	3.1	0	0	0	0	0
NAEI (2018)		18.4	13.1	5.2	28.8	124.9	30.3	n.a.				
EEMS (2018/2019)	all	18.4 / 12.1	13.1 / 7.9	9.2 / 9.3	27.1 / 58.6 ᵃ	19.6 / 19.6 ᵇ	22.3 / 18.3	n.a.				
	turbines, engines	0.4 / 0.4	0.5 / 0.4	4.7 / 4.7	3.8 / 5.5	11.4 / 8.2	0.01 / 0.7					
	fug	3.9 / 0	6.1 / 0	n.a. / n.a.	0 / 0	4.5 / 4.6	0					
	vent	14.0 / 11.6	6.5 / 7.5	4.5 / 4.6	23.3 / 53.1	3.8 / 6.8	22.3 / 17.7					
	flar	0 / 0	0 / 0	0	0 / 0	0 / 0	0					
Reporting by operators (survey date)		n.a.						133.8 vent + fug	17.3 vent + fug	0.03 ᶜ vent + fug	41.7 vent, no flar	0 no vent, no flar
Ship observation (11/2018) (Hensen et al., 2019)		n.a.						126 - 194.4	29.9 - 72	not sampled	50.4 - 252	10.4 - 18.4

ᵃ reporting for 2 (2018) and 1 (2019) platform out of 19 platforms. ᵇ reporting for 1 (2018 and 2019) platform out of 15 platforms. ᶜ P9: offline (no dry gas production)

3.1.1 Comparison to a globally gridded annual inventory (Tier 1)

We compare our estimated fluxes with the GFEI v2 for 2019, which contains total CH_4 emissions from fossil fuels exploitation
and a distribution of emissions per subsector. The platforms surveyed in this study are considered to be processing, production
and exploration sites by the inventory. As an example, the total CH_4 emissions reported for P1 (2.9 kg h^{-1}) break down to: 44%
estimated to arise from fugitives during gas processing, 43% from flaring during gas processing, 10% from exploration
(fugitives + venting + flaring emissions) and 4% from flaring during production. According to the inventory, UK emissions
are fugitive, venting and flaring emissions, whereas emissions on Dutch sites arise only from flaring. For all sampled
installations, operations other than exploration, production and processing are claimed to emit no CH_4.

Compared to the GFEI v2 data set for total CH_4 emissions from gas exploitation, the measured fluxes of (1369.4 ± 568.3) kg h^{-1} are 21 times higher than GFEI data (65.9 kg h^{-1}) for all sampled UK facilities on aggregate. However, the highest emitting
UK site (P4 complex) is identified as the highest emitter by the GFEI, as well. The factor by which measured emissions around
Dutch sites are underestimated by the GFEI is an order of magnitude higher compared to UK sites: Measured fluxes
$((122.9 \pm 36.8)$ kg h^{-1})) are 279 times higher than GFEI data (0.44 kg h^{-1}) on aggregate for all sites. This high discrepancy
points to the weaknesses in using global inventories for field-specific emissions characterisations especially when compared
with snap-shot measurement studies. However, similar to UK sites, the two platforms (P7, P8) with highest emissions measured
are correctly identified by the GFEI as the highest emitters.

For the sampled installations in this study, Dutch GFEI data is two orders of magnitude smaller compared to UK GFEI data.
GFEI relies on UNFCCC reported emissions. Using the UNFCCC GHG Data Interface (UNFCCC, 2022), Dutch annual CH_4
fugitive emissions from the natural gas energy production sector and reported for the year 2019 are 14 times smaller compared
to the UK equivalent. Further, in contrast to UK reporting, no data is reported for the natural gas subsectors exploration,
production and processing. Thus, GFEI values for Dutch sites can only arise from UNFCCC reported total venting and flaring
emissions, since those are disaggregated by the inventory to the subsectors. For the sampled Dutch sites in this study, the
inventory gives only flaring emissions from production and processing. Therefore, the UNFCCC reported Dutch emissions,
which the inventory is based on, could explain the high discrepancy between GFEI Dutch and UK values.

A related study of 21 oil and gas facilities in the Norwegian Sea finds a better agreement of the GFEI v1 (2016) with the
measured fluxes being only a factor 1.4 higher in aggregate for all platforms (Foulds et al., 2022). Similar to the Dutch
UNFCCC reporting, the Norwegian UNFCCC reporting does not show emissions for the natural gas subsectors exploration,
production and processing. Considering that Foulds et al. sampled both oil and gas producing installations, the better agreement
could possibly be attributed to UNFCCC reported emissions for the oil sector.

3.1.2 Comparison to UK annual point-source inventories

The annual estimates of the UK national point-source inventories NAEI and EEMS are smaller than the fluxes measured during this study. The measured fluxes for P1 and P4 are underestimated, while P2 agrees with both inventories within uncertainties. For 2018 the measurement-derived fluxes are a factor of ~6 (NAEI; 220 kg h^{-1}) and ~12 (EEMS; 109.7 kg h^{-1}) higher cumulatively for all sampled facilities. However, EEMS emission data for 2019 agree slightly better with the observations taken in 2019: Top-down estimates are a factor of ~11 higher compared to the EEMS reported data (125.8 kg h^{-1}). Most CH$_4$ emissions of sampled installations and reported by EEMS are attributed to venting (35% - 96%) besides emissions arising from the operation of turbines and engines (0.1% - 50%). It is worth noting that for all platforms listed in EEMS, zero flaring emissions are reported. During the flights no visible flaring was observed. Nevertheless, flaring is stated to have a share of 3% of the Southern North Sea region's total CH$_4$ emissions in 2019 (OGA, 2020). The Global Gas Flare Catalog 2019 from the Earth Observation Group at the Payne Institute for Public Policy (Elvidge et al., 2015; Elvidge et al., 2013), which uses VIIRS data, shows flaring in the North Sea region. However, for the sampled installations no flaring is observed in 2019, which confirms the inventories zero flaring claim at least for the sampled installations.

As discussed in section 2, EEMS data is fed into the NAEI inventory, hence we expect that NAEI 2018 reported values are the same or higher than EEMS 2018 data. A comparison between NAEI data and EEMS data from 2018 shows that NAEI numbers are consistent with EEMS for two (P1, P2) and higher than EEMS data for three (P4, P5, P6) UK platforms. However, for P3 the NAEI reported value is smaller compared to EEMS 2018. This could either indicate an error in the EEMS reporting or it might be that the emissions of P3, which consists of 3 platforms, are misallocated in the NAEI.

In EEMS emissions are listed for one specific platform, also in the case of multi-platform complexes (P4, P5). Those platforms might be interpreted as being representative platforms with the reported emissions being aggregated emissions for the complex. Regarding the multi-platform complex P4, we used the FLEXPART (FLEXible PARTicle) dispersion model (Pisso et al., 2019) to attribute the measured emission plumes to individual platforms located within the complex (see Appendix C). The platforms that the observed fluxes were attributed to do not match with the (representative) platforms listed in EEMS 2018/2019.

The discrepancy to UK national inventories detected in this study is higher than reported in previous airborne studies of other offshore regions. Zavala-Araiza et al. (2021) estimated offshore CH$_4$ emissions in the Sureste Basin, Mexico, to be more than an order of magnitude lower than the values given in the Mexican greenhouse gas emission inventory. Gorchov Negron et al. (2020) generated an airborne measurement-based inventory comprising offshore facilities located in the U.S. Gulf of Mexico. They showed that for shallow-water facilities CH$_4$ emissions are more than a factor of two higher than the estimate of the U.S. Environmental Protection Agency Greenhouse Gas Inventory (EPA GHGI) and the Gulfwide Offshore Activity Data System (GOADS) inventory.

3.1.3 Comparison to facility-level reporting by platform operators for the survey date

As expected, the smallest discrepancy between top-down and bottom-up estimates exists for the comparison with emission data of individual facilities provided by platform operators for the specific survey day. Operator-based reporting was only available for the five sampled Dutch installations (P7-P11). The facility-level estimates deviate by up to a factor of ~12 compared to the reporting, whereby two out of five facilities (P7, P10) are overestimated and another two facilities underestimated (P8, P11). P9 is reported as offline on the survey day, which agrees with the measurements showing no elevated CH_4, C_2H_6 and CO_2. According to the operators, CH_4 emissions arise from venting and fugitives for 4 out of 5 installations (P7-P10). P10 is reported as offline during the time of flight, while emissions are still measured and smaller than the reported venting CH_4 emissions. For P11 no venting or flaring was recorded, although CH_4 was detected during the measurements conducted downstream. The measured emissions might be attributed to fugitives, which are not excluded by the operator in this case. Flaring emissions are explicitly excluded only for two out of five installations (P10, P11). For P7-P9 flaring emissions could contribute, though. For all sampled Dutch installations together, we find that our estimated flux of (122.9 ± 36.8) kg h^{-1} deviates by a factor 0.64 (ranging from 0.33-12 for individual facilities) from reported values (192.8 kg h^{-1}). A comparison with operator-reported data for offshore installations in the Norwegian Sea by Foulds et al. (2022) shows that although there are deviations for individual facilities, reported data agree similarly well on aggregate for a larger sample size (18 facilities) with the measured fluxes being smaller than reported emissions by a factor 0.8 (ranging from 0.1-22 for individual facilities).

3.1.4 Comparison to a ship-based top-down study

The planning for the flight on 2019/05/06 around Dutch installations relied on a ship-based top-down study conducted by the Netherlands Organisation for Applied Scientific Research (TNO) in 2018 (Hensen et al., 2019). With the aim to derive CH_4 emission fluxes, measurements were taken at distances up to ~3 km downwind of 33 platforms in November 2018. CH_4 was measured with a TILDAS spectrometer (Aerodyne Research, Inc.) and a Picarro instrument, whereby the inlet was installed at 35 m above sea level. The results shown in Table 1 were obtained by combining the measurements with a Gaussian plume model and a tracer-release experiment. The derived fluxes range from 10 kg h^{-1} to 252 kg h^{-1}. For P8 and P11 our fluxes are within the range of the determined fluxes from the ship-based study, whereas in case of P7 and P10 our measured fluxes are smaller. For the studied 4 Dutch facilities in aggregate, our measured fluxes ((122.9 ± 36.8) kg h^{-1}) are smaller with respect to the ship-based measurements (216.7 kg h^{-1} - 536.8 kg h^{-1}) and deviate by factor 0.23-0.57.

3.2 Correlation between CH_4 and C_2H_6 for all platforms

For all sampled installations for which enhanced CH_4 was detected, we observe clear correlations with co-emitted C_2H_6, which is an indicator for fossil fuel emissions (Lowry et al., 2020; Peischl et al., 2018; Hausmann et al., 2016; Smith et al., 2015). C_2H_6 to CH_4 ratios of fossil fuels depend on the type of field/reservoir (gas, gas condensate, oil). Since the Southern North Sea region contains predominantly dry gas fields with relatively low gas condensate (wet gas) production, we expect low C_2H_6 to

CH$_4$ ratios ranging from 1-5% (dry gas) and 5-10% (gas condensate) (Xiao et al., 2008, Jones et al., 1999) or 1-6% (dry gas) and > 6% (wet gas) (Yacovitch et al., 2014, Whiticar et al., 1994). We calculate an C$_2$H$_6$ to CH$_4$ ratio for each transect from the integrated plume area of the respective CH$_4$ and C$_2$H$_6$ enhancement, and take the average over all transects for each sampled installation. As an example for the calculation, Figure A2 (b) in the Appendix A shows the simultaneous enhancements in C$_2$H$_6$ and CH$_4$ for peak 5 of P1. Measured values range from 2.5% to 7.8% for all installations. We compare the measured ratios to reported values from the OGA Shell/ExxonMobil Geochemistry Database for Central North Sea (2017) for UK sites and the NLOG for Dutch sites (for all measured and reported values see Table D1 in the Appendix D). Compared to the measured ratios, the reporting underestimates the measurements for P7 and P10 and overestimates the measured value for P11, but is consistent for P4 and P8. In general, the dry gas and gas condensate binary categorization matches for the observed and reported ratios.

3.3 Correlation between CH$_4$ and CO$_2$ for selected platforms

Enhanced CO$_2$ mole fractions accompanied the CH$_4$ enhancements at five installations (P1, P2, P4, P7, P10) indicating a combustion source from either flared CH$_4$ or other combustion sources such as turbines or engines. For P8 and P11 C$_2$H$_6$ was enhanced while no CO$_2$ enhancement was observed (< LoD). Figure 3 shows the time series for a transect flown downwind of P1 with simultaneous enhancements in CH$_4$, CO$_2$ and C$_2$H$_6$ mole fractions as an example of the observed plumes. The CO$_2$ flux is determined from the gradient of a linear regression between the CO$_2$ and CH$_4$ enhancements since both species are detected by the same instrument (Picarro Analyser). Figure A2 (a) in the Appendix A shows the CH$_4$ to CO$_2$ scatter plot for P1. For three of the platforms (P1, P4, P10), CH$_4$ and CO$_2$ were well-correlated and CO$_2$ fluxes have been determined.
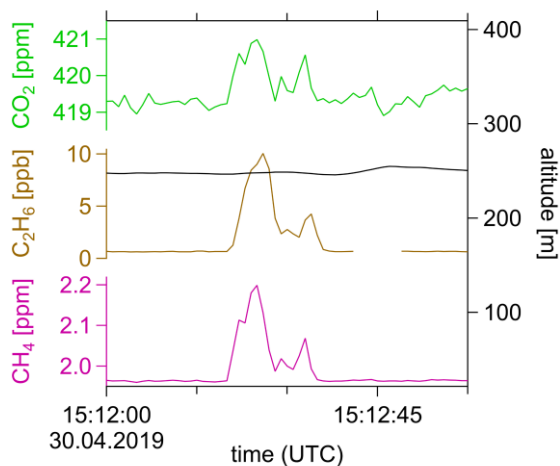
Figure 3. Time series (1 Hz) of a transect at 250 m altitude downwind of P1: Coinciding elevations in CO_2 (green), C_2H_6 (brown) and CH_4 (magenta) mole fractions. C_2H_6 is a tracer for fossil fuel emission and CO_2 indicates a combustion source.

Table D1 in the Appendix D shows the measured CO_2 fluxes along with inventory emission data from the UK point-source inventories NAEI and EEMS and Dutch operator data. For P1 EEMS 2018 and 2019 overestimate emissions, while the NAEI

350   inventory states lower emissions, but matches within the uncertainties. Likewise, EEMS 2019 agrees within the uncertainties with measured CO_2 fluxes from P4, while both NAEI and EEMS 2018 underestimate emissions. According to EEMS, which categorizes emissions into turbines/engines, fugitives, venting and flaring, CO_2 emissions arise mainly from the combustion of diesel and gas in turbines and engines. Only for the platform complex P5 minor emissions from fugitives and venting are listed. In EEMS flaring emissions are zero for all UK platforms. This is inconsistent with data from the UK Oil and Gas

355   Authority, which reports that 4% of CO_2 emissions in the SNS region are supposed to arise from flaring in 2019 (OGA, 2020). From the amount of CO_2 and CH_4 flaring emissions in 2019 in the SNS and Irish Sea region given in the Flaring and Venting Report (OGA, 2020), the unburnt fraction, i.e. the ratio of unburnt CH_4 to CO_2 from flaring emissions, is 6.4%. If we calculate this ratio for the sampled CH_4 and CO_2 plumes at the UK platforms, we get higher ratios: 12.4% (P1) and 14.7% (P4). This means that either there is no flaring on the platform, or if some flaring occurred, there were additional CH_4 fugitive or venting

360   sources. Comparing to Dutch operator data, we find that around two Dutch platforms (P8, P11) no simultaneously emitted CO_2 was detected, although Dutch operator data states CO_2 emission on the survey date. For P10 we derive a CO_2 flux half the size of the emissions reported for the survey date. Dutch operator data explicitly excludes flaring sources for P10 and P11 (see Table 1) and lists only combustion sources such as turbines and engines. To sum up, from the measured total emissions we cannot clearly differentiate flaring from other combustion sources. But if there were any flaring sources, there must have been

365   additional fugitive/venting CH_4 sources according to the measured CH_4 to CO_2 ratios.

3.4 Loss rates

In this section we determine loss rates, i.e. the ratio of gas lost to the atmosphere to dry gas production rates. We calculate the amount of gas lost to the atmosphere from the determined CH_4 emission rates and the CH_4 mol % from the OGA Shell/ExxonMobil Geochemistry Database for Central North Sea (2017) for UK sites and from the operator data for Dutch sites. UK production rates are given as monthly values by OGA. We include production from upstream fields with only subsea wells and no platform infrastructure. Dutch production data was provided by Dutch operators for the specific survey day. For three UK facilities (P3, P5, P6) no emissions were detected, although they were producing during the month of survey. According to the Dutch operator, P9 did not produce on the survey day, and we did not detect a plume either.

Determined loss rates for Dutch and UK sites are smaller than 1.0%, except for P4, which shows an higher loss rate of 3.1% (see Appendix E for individual production rates and loss rates). Besides the fact, that P4 is a multi-platform complex and relatively old, i.e. producing since 50 years, there is no indication of abnormal activities on the survey date.

3.4.1 Comparison with airborne studies in other regions (Norwegian Sea, Northern Gulf of Mexico)

Figure 4 depicts the determined CH_4 emission rates and production rates from this study compared to the results obtained in two other airborne studies conducted by Foulds et al. (2022) in the Norwegian Sea and Gorchov Negron et al. (2020) in the Northern Gulf of Mexico.
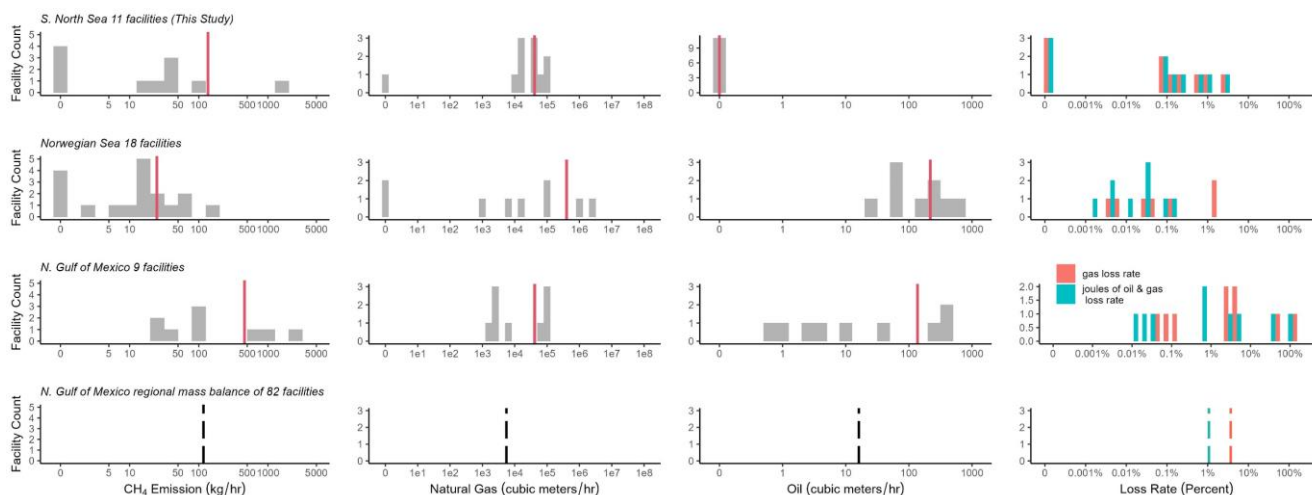
Figure 4. Comparison of measured CH_4 emission rates (first column), corresponding natural gas (second column) and oil (third column) production rates and loss rates (fourth column) in the Southern North Sea (this study) with two other airborne studies conducted in the Norwegian Sea (Foulds et al., 2022)) and in the Northern Gulf of Mexico (Gorchov Negron et al., 2020). Red lines denote the respective average values. The dotted lines show the average value obtained in a regional mass balance in the Northern Gulf of Mexico. The facility count does not include satellite structures.

The CH$_4$ emission fluxes for individual facilities, i.e. rates, calculated in this study compare to the emission rates determined in the Norwegian Sea and in the Northern Gulf of Mexico (see left side of Figure 4). The emission rate of P4 is as high as the emissions measured around similar infrastructure types in the Northern Gulf of Mexico, i.e. multi-platform complexes in shallow water, which equally show emission rates higher than 500 kg h^{-1}. In the Gulf inconstant temporal variability of those infrastructure types was seen, what might correspond to the non-detectable emissions of the multi-platform complex P5. Comparing average absolute emission rates per facility (red vertical lines), the lowest average emission rates were determined around 18 facilities in the Norwegian Sea (24 kg h^{-1}) and highest emission rates around 9 facilities in the Gulf (457 kg h^{-1}) with a factor of 19 difference. Our average emission estimate in the Southern North Sea is 136 kg h^{-1} and compares well with the average absolute emission rate in a regional mass balance in the Gulf with a larger sample size (117 kg h^{-1}). When excluding the multi-platform complex P4, the Southern North Sea average emission estimate amount to 23 kg h^{-1}, which compares well with the average emission rate in the Norwegian Sea, where no multi-platform complex was sampled.

In contrast to the Southern North Sea, where gas (with little gas condensate) production dominates, in the Northern Gulf of Mexico natural gas is produced as a side product from oil exploitation (associated gas) and in the Norwegian Sea both oil and gas production takes place. The natural gas production rates for the facilities in the Southern North Sea shown in the second column in Figure 4, are on average one order of magnitude smaller than in the Norwegian Sea and one order of magnitude higher than in the Gulf regional estimate, but almost the same value as the Gulf facility-wise estimate. Average oil production rates in the Norwegian Sea and in the Northern Gulf of Mexico are comparable.

Total loss rates, i.e. all gas lost to the atmosphere divided by total production rates in the respective region, can be determined either from gas production only or from the sum of oil and gas production. Thereby, we convert oil and gas production rate units according to the energy content. Considering only gas production, the total loss rate in the Southern North Sea (0.54% (0% - 3.1%)) is one order of magnitude higher than in the Norwegian Sea (0.02% (0.003% - 1.6%)) and one order of magnitude smaller than in the Gulf. The latter amount to 1.9% (0.04% - 128%) for the facility-level measurements and 3.7% for the regional measurements. Including oil production, total loss rates in the Norwegian Sea (0.01% (0.001% - 0.2%)) and in the Gulf (0.51% (0.01% - 112%) for the facility study; 1.1% for the regional study) are reduced. Thus, total loss rates in the Southern North Sea and in the Gulf compare to each other, when including oil production, and total loss rates in the Norwegian Sea are still one order of magnitude smaller compared to the other regions, but span over 3 orders of magnitude.

4 Conclusion

We report CH$_4$ flux estimates for six UK and five Dutch offshore gas production installations in the Southern North Sea derived from airborne measurements conducted in spring 2019. We identified the observed CH$_4$ enhancements as emissions arising from natural gas based on co-emitted C$_2$H$_6$ and derive C$_2$H$_6$ to CH$_4$ ratios for each offshore installation. Comparison with a ship-based top-down study conducted around Dutch facilities in 2018 (Hensen et al., 2019) shows that our derived CH$_4$ fluxes

deviate by a factor 0.23-0.57 being smaller with respect to fluxes derived by Hensen et al. Our CH_4 flux estimates were compared with different bottom-up inventories available for this region, including the Global Fuel Exploitation Inventory

415 (GFEI) (Scarpelli et al., 2019), the UK Environmental and Emissions Monitoring System database (EEMS), the UK National Atmospheric Emissions Inventory (NAEI), and direct facility-level reporting by Dutch operators. In general, the comparison for individual facilities shows a large discrepancy between the top-down derived emissions and all bottom-up (inventory and reported) estimates, which may be expected because of the nature of single snap-shot measurements per facility in this study and potential temporal variability per facility demonstrated via repeat measurements by Foulds et al. (2022). The largest

420 discrepancy exists with the annual emission data from the globally gridded GFEI inventory for the year 2019, showing that measured aggregated emissions from UK and Dutch sites are higher by a factor of ~ 21 and ~ 279, respectively. On the one hand, these high discrepancy factors reflect the weaknesses in using global inventories based on Tier 1 methods for field-specific emissions characterizations, especially when comparing with snap-shot measurements. On the other hand, Dutch UNFCCC reported emissions, which the inventory is based on, are much smaller compared with UK UNFCCC reporting and

425 could give rise to the exceptionally large factor for Dutch sites. Our top-down emission fluxes for all sampled UK installations in aggregate deviate from UK national annualized emission data from NAEI and EEMS for the year 2018 by factors of 6 and 12, respectively. NAEI inventory data, which is based on EEMS operator-based reported, is equal to or higher than EEMS, except for one out of six installations. Latest UK national inventory data available for 2019 from EEMS deviate slightly less from the measurements with the latter being a factor 11 higher for all sampled UK facilities in aggregate. According to the

430 EEMS inventory, CO_2 emissions measured around UK facilities and correlating with CH_4 emissions are solely attributable to combustion sources (turbines, engines) while flaring emissions are reported as zero for both CO_2 and CH_4. The measurements in this study cannot differentiate flaring from other combustive sources, and thus rule out flaring. Still, the measured ratios of emitted CH_4 to CO_2 point at existing venting/fugitive CH_4 sources, whereby flaring sources could be contributing.

As expected, the best agreement with our flux estimates exists with facility-level reporting from Dutch operators for the specific

435 survey date. The measurements deviate by a factor of 0.64 (0.33-12) and are smaller with respect to Dutch reported emissions for all sampled facilities in aggregate. Our results for operator-based facility-level reporting compare very well to a study conducted in the Norwegian Sea by Foulds et al. (2022), which find their measurements deviating by a factor 0.8 and being smaller compared to the reporting by operators. We conclude that for sites with operator-based facility-level reporting in Dutch waters, – as suggested in the reporting framework Oil and Gas Methane Partnership 2.0 (www.ogmpartnership.com) – the

440 highest accuracy is demonstrated compared to measurements. The adoption of facility-level estimation in national inventories would be expected to increase the accuracy of national CH_4 emissions accounting for the offshore oil and gas sector. To improve comparisons of top-down and bottom-up observation and resolve discrepancies, generating bottom-up inventories at facility-scale and accounting for temporal variability when including top-down measurements would be extremely valuable.

A regional comparison to airborne studies in the Norwegian Sea (Foulds et al., 2022) and in the Northern Gulf of Mexico (Gorchov Negron et al., 2020) shows that the absolute facility-level emission rates agree with the general distribution found in other offshore basins. This is despite differing gas production rates, which span two orders of magnitudes across geographies. Including oil production rates, total loss rates of the Southern North Sea compare to total loss rates in the Gulf, whereas loss rates in the Norwegian Sea are one order of magnitude smaller. As a consequence of the similar absolute emission rates, mitigation is needed virtually equally across geographies. Further, average absolute emission rates in this study are substantially larger in the UK compared to NL, which is largely driven by one super-emitter in the UK. The emission of the super-emitter is as high as the emissions measured around similar infrastructure types (multi-platform complexes in shallow water) in the study in the Northern Gulf of Mexico, but additional sampling in future studies is needed to investigate representativeness.

Appendices

A. Example for flux calculation for P1

In the following, the CH_4 flux calculation is illustrated by using observations of platform P1 on 30 April 2019. Measurements were performed downwind at a distance of around 3-4 km from the platform (wind direction (179.5 ± 29.8) °; perpendicular wind speed $V_\perp = (3.2 \pm 1.5)$ m/s). To fully capture the emitted CH_4 plume dispersed within the boundary layer, which extended up to (420 ± 20) m, vertically stacked transects were flown between 97 m and 305 m. Figure A.1 shows the downwind horizontal transects with CH_4 mole fractions color-coded in panel (a) and the corresponding time series in panel (b). CH_4 enhancements were detected in all seven transects. We calculated CH_4 fluxes for each transect resulting in a total flux of (86.5 ± 41.2) kg h^{-1}. The uncertainty is given for confidence intervals of 1 standard deviation and arises mainly due to wind measurements. CO_2 fluxes are calculated using the slope of the linear regression between co-emitted CO_2 and CH_4 for the respective peaks. Panel (a) in Figure A.2 shows the scatter plot for CO_2 and CH_4 for platform P1, where enhanced CO_2 was found for two peaks at altitudes above 240 m. The observation of co-emitted CO_2 points to a buoyant plume adding up to the CH_4 plume at altitudes above 240 m. Panel (b) in Figure A.2. shows the time series of measured CH_4 and C_2H_6 for the transect at 250 m altitude downwind of P1 to illustrate the calculation of the C_2H_6 to CH_4 (C2:C1) ratio. The peak areas for C_2H_6 and CH_4 enhancements over the background are shown in yellow. The C2:C1 ratio is calculated by dividing the integrated peak area of C_2H_6 by the integrated peak area of CH_4, which results in a C2:C1 ratio of 4.3% in this case.
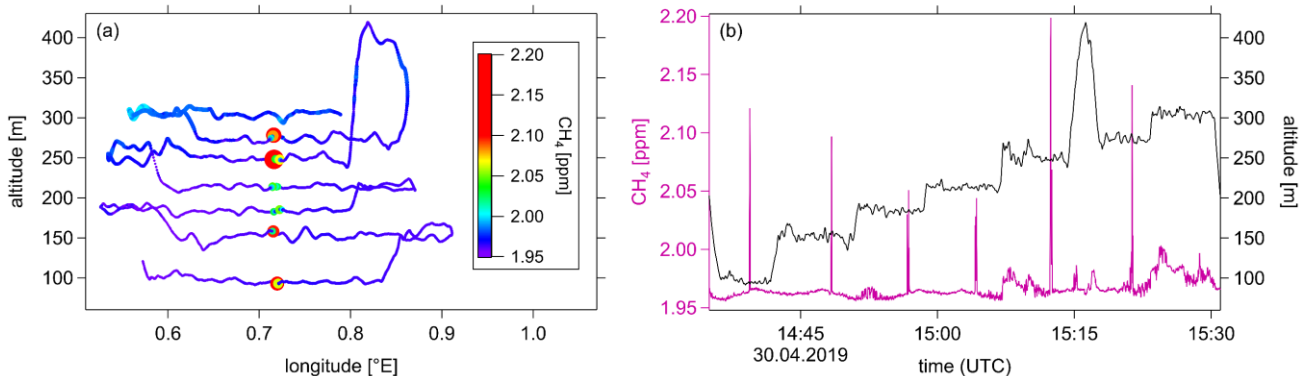
Figure A1. Example for measurements downwind of platform P1 during the offshore flight on 30 April 2019: (a) horizontal transects at altitudes between 94 m and 304 m above sea level. CH_4 enhancements are elucidated with a color-scale, whereby the size of plotted symbols is scaled to CH_4 mole fractions. (b) corresponding CH_4 time series.

470
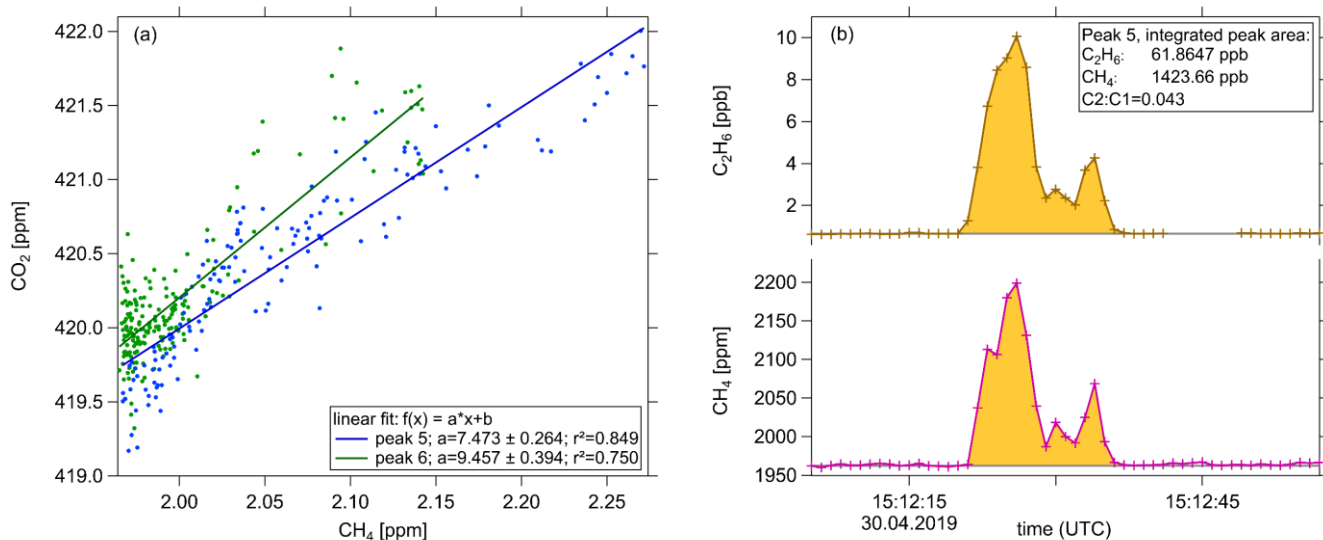
Figure A2. (a) Scatter plot for co-emitted CO_2 downwind of platform P1. Enhanced CO_2 was found for two peaks at altitudes above 240 m. (b) Time series (1 Hz) of the transect at 250 m altitude downwind of P1 (peak 5): Coinciding elevations in C_2H_6 (brown) and CH_4 (magenta) mole fractions. The C_2H_6 to CH_4 (C2:C1) ratio is calculated from the fraction of the integrated peak areas (yellow) over the background mole fractions (gray) and over the time span of the peak (18 s).

B. Uncertainty analysis for flux calculation

We use the Gaussian error propagation to determine the uncertainty of the flux calculation, represented as confidence intervals of 1 standard deviation (see eq. (1) in subsection 2.2). The uncertainties of the calculated CH_4 fluxes for each layer i result

475 from the uncertainties of each measured parameter q (eq. B1). These parameters are the elevated CH_4 mole fractions ΔC_i, wind

speed $V_\perp$, pressure p_i, temperature T_i, plume width Δx_i and plume height D_i. The total uncertainty is the sum of the uncertainties of the fluxes calculated for each transect (eq. B2).

$$u(Flux_i) = \overline{Flux_i} \cdot \sqrt{\sum_q^{parameters} \left(\frac{u(q)}{\bar{q}}\right)^2} \tag{B1}$$

$$u(Flux_{total}) = \sum_i^{transects} u(Flux_i) \tag{B2}$$

480   The beginning of the plume is defined as a measured concentration enhancement that is higher than 2 standard deviations of the background mole fractions. For ΔC_i the CH$_4$ mole fractions measured in- (C_i) and outside (C_0) of the plume are used. Both C_i and C_0 have a systematic uncertainty resulting from the Picarro instrument uncertainty of 1.2 ppb (France et al., 2021). The background mole fraction at each point j within the plume is determined from an interpolation between $C_{0,a}$ and $C_{0,b}$, which are the mean CH$_4$ mole fractions within 30 s before and after the plume. The uncertainty of the interpolated background at

485   each point $u(\Delta C_{0,j})$ is calculated from the standard deviations $\sigma_{0,a}$ and $\sigma_{0,b}$ of $C_{0,a}$ and $C_{0,b}$ (eq. (B4)). The parameter n denotes the number of points within the plume.

$$u(\Delta C_i) = \sqrt{\sum_a^b (u(C_{i,j})^2 + u(C_{0,j})^2)} \tag{B3}$$

$$u(\Delta C_{0,j}) = \sqrt{(\sigma_{0,a} \cdot \frac{n_i - j}{n_i})^2 + (\sigma_{0,b} \cdot \frac{j}{n_i})^2} \tag{B4}$$

We determine the perpendicular wind speed from the average aircraft heading, measured average horizontal wind speed and

490   average wind angle over all transects. The uncertainty of the perpendicular wind speed $u(V_\perp)$ is a result of the standard deviations and valid for all transects:

$$u(V_\perp) = \sqrt{\left(\frac{\partial V_\perp}{\partial\, heading} \cdot \sigma_{heading}\right)^2 + \left(\frac{\partial V_\perp}{\partial\, wind\, speed} \cdot \sigma_{wind\, speed}\right)^2 + \left(\frac{\partial V_\perp}{\partial\, wind\, angle} \cdot \sigma_{wind\, angle}\right)^2} \tag{B5}$$

For the uncertainties of pressure $u(p_i)$ and temperature $u(T_i)$ the standard deviations of the mean values across the plume and the 30 s background are taken.

495   The plume width is determined by the distance the aircraft covered while crossing the plume. Thereby, the velocity of the aircraft is multiplied with the time span of the plume. The uncertainty of the plume width $u(x_i)$ is derived from the uncertainty (standard deviation) of the measured velocity of the aircraft.

Since we assume a well-mixed plume within the boundary layer, the uncertainty of plume height $u(D_i)$ is characterized by the uncertainty arising from the estimation of the boundary layer height. Therefore, $u(D_i)$ is only relevant for the uncertainty of

500   the flux calculated for the uppermost layer.

The uncertainty of the wind measurement is the biggest contributor to the total uncertainty of the flux calculation (typically 90%). Uncertainties of wind speed and wind direction measurements range from 1-3 m/s (23-70% relative uncertainty at 1σ)

and 8-39° (2-19% relative uncertainty at 1σ), respectively. The uncertainty of plume height ranges from 20-32 m and accounts for less than 10% of total uncertainty of the flux calculated for the uppermost layer.

505 **C. FLEXPART Dispersion Model: Example footprint analysis for the multi-platform complex P4 (backward simulation)**

The model study concludes, that 9 out of 19 platforms of the complex could have contributed to the measured CH_4 enhancement (flight track with color-coded CH_4 in Figure C1). None of the possible emitters is listed in the inventories as single platforms.
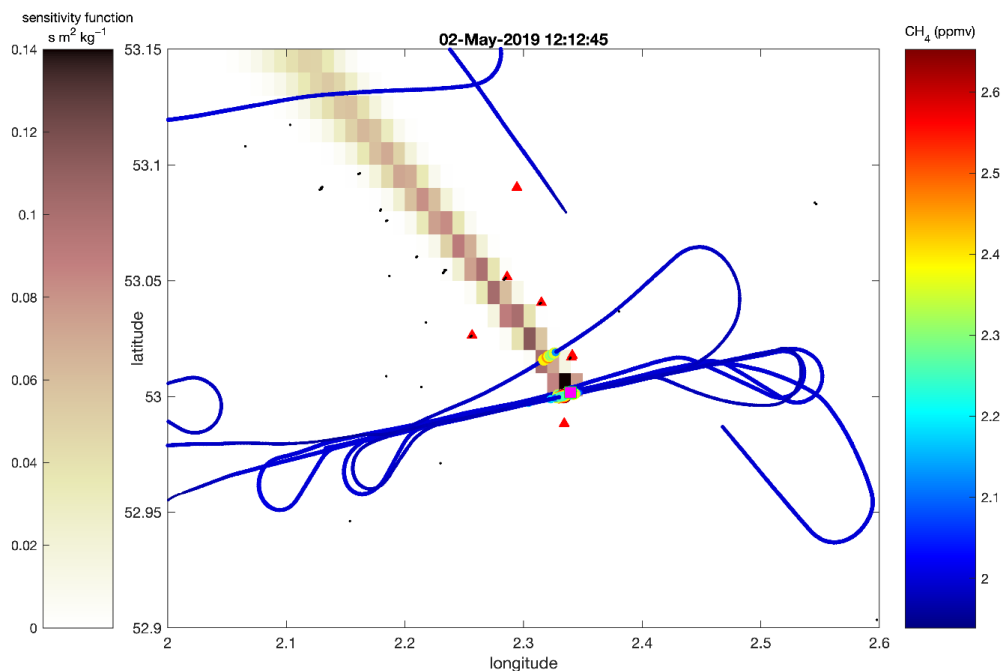
Figure C1: Footprint analysis for the multi-platform complex P4 (backward simulation) sampled during flight 327: The flight track is shown with color-coded CH_4 in units of ppm. The particle density is shown with a brownish scale. Black markers symbolize the installations in the area and red markers show all installations which could have contributed to the measured plume.

510 **D. Comparison of C_2H_6 to CH_4 ratios and CO_2 fluxes with reported values**

Table D1. Measured and reported (OGA, NLOG) C_2H_6 to CH_4 ratios for all sampled platforms at 2σ. All installations for which CH_4 was enhanced were accompanied by co-emitted C_2H_6. No detected C_2H_6. C_2H_6 and CO_2 enhancements are indicated with $<$ LoD. Measured CO_2 emissions are compared to UK inventory data (NAEI, EEMS) and Dutch operator data. Information on emission processes is given for venting (vent), fugitives (fug) and flaring (flar). CO_2 emissions are rounded to two significant digits.

		P1	P2	P3	P4	P5	P6	P7	P8	P9	P10	P11
Survey date		30 April 2019			2 May 2019			6 May 2019				
Country		UK			UK			NL				
Installation		P1	P2	P3	P4 complex	P5 complex	P6 complex	P7	P8	P9	P10	P11
C_2H_6/CH_4 [%]	This study	4.3 ± 0.2	2.5 ± 1.1	< LoD	2.8 ± 0.4	< LoD	< LoD	5.6 ± 0.5	4.3 ± 0.9	< LoD	7.8 ± 1.0	5.3 ± 0.7
	OGA/NLOG	n.a.	n.a.	3.3	3.2	4.9	4.3	3.3	3.6	4.3	6.0	6.1
CO_2 flux [kg/h]	This study	640 ± 300	weak correlation	< LoD	21850 ± 8870	< LoD	< LoD	weak correlation	< LoD	< LoD	5290 ± 1580	< LoD
	NAEI (2018)	410	390	200	3110	4160	1070			n.a.		
	EEMS (2018/2019) all	1490 / 1490	1430 / 1210	740 / 740	11400 / 17110	15260 / 11880	3930 / 2180			n.a.		
	turbines, engines	1490 / 1490	1430 / 1210	740 / 740	11400 / 17110	15260 / 11880	3930 / 2180					
	fug	0 / 0	0 / 0	n.a. / n.a.	0 / 0	0.07 / 0.05	0 / 0					
	vent	0 / 0	0 / 0	0 / 0	0 / 0	0.07 / 0.08	0.02 / 0.02					
	flar	0 / 0	0 / 0	0 / 0	0 / 0	0 / 0	0 / 0					
Reporting by operators		n.a.						16520 turbines, furnaces, vent	330 turbines, vent	0	10690 turbines, power generators	570 Turbines, engines, furnaces, diesel

E. Production rates and loss rates (including non-emitting installations)

Figure E1 shows gas lost to the atmosphere, which is calculated from CH_4 emission rates and the CH_4 mol % (UK sites: OGA
Shell/ExxonMobil Geochemistry Database for Central North Sea (2017); NL sites: operator data). The determined loss rates
are the ratio of gas loss and dry gas production, i. e. normalized CH_4 emissions against natural gas production rates.

Table E1 shows platform production rates along with calculated loss rates. No loss rates were determined for installations,
where emissions were below detection limit and thus, no enhancements measured (abbreviation "no enh."). Z1-Z8 are non-
emitting installations from fly-bys. Individual platform production data for 2019 were taken from the UK Oil and Gas Authority
(OGA), the NLOG and operator reported data. UK production rates are given as monthly values by OGA. Thereby, we include
production from upstream fields with only subsea wells and no platform infrastructure. Dutch production data was provided
by Dutch operators for the specific survey day.
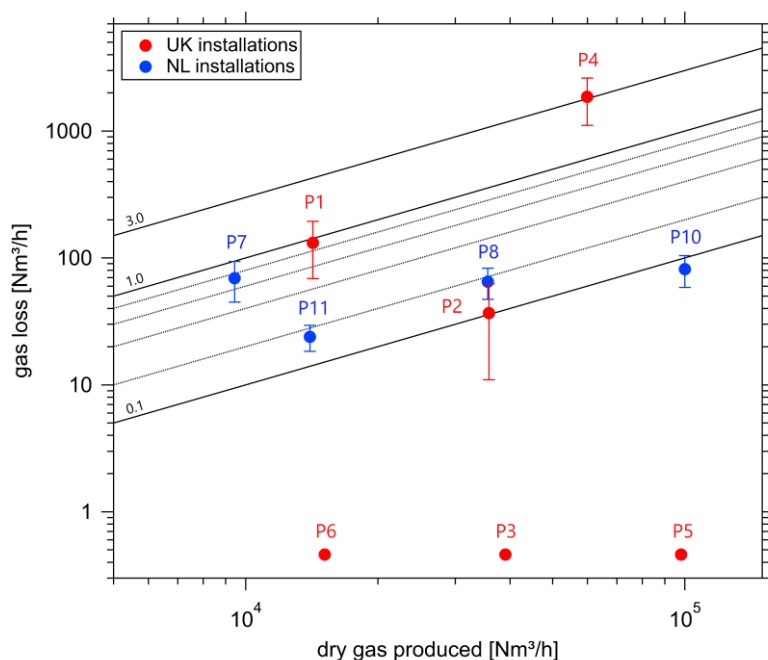
Figure E1. Gas lost to the atmosphere against the amount of dry gas produced in norm cubic meters (Nm^3) per hour (UK: OGA, NL: operator data). Dutch platforms are shown in blue, UK platforms in red. Note that no downwind enhancements were detected for 4 installations (P3, P5, P6, P9) with only P9 (NL installation, excluded) not producing. Lines of constant loss rates (%) are shown in black.

Table E1. Reported production rates and calculated loss rates for sampled UK (P1-P6) and Dutch (P7-P11) installations. Z1-Z8 are (non-emitting) installations from fly-bys.

facility	Dry gas production (OGA (UK), NLOG (Dutch)) [Nm³/month]	Operator reported gas production [Nm³/day]	loss rate [%]	Start of production [yr]
P1 [a]	10238885 (+ 98 Nm³ gas condensate)	n.a.	0.92 ± 0.42	1988
P2 [b]	25765475	n.a.	0.10 ± 0.07	1990
P3	28090814 (+ 44 Nm³ gas condensate)	n.a.	no enh.	1967
P4 [b]	44571997 (+ 194 Nm³ gas condensate)	n.a.	3.10 ± 1.19	1968
P5	72934875 (+ 72 Nm³ gas condensate)	n.a.	no enh.	1968
P6 [b]	11259835 (+ 150 Nm³ gas condensate)	n.a.	no enh.	1969
P7	855993	226383	0.73 ± 0.27	1977
P8	11049455	854000	0.18 ± 0.05	1983
P9	0	0	no enh.	1991
P10	28340954	2400000 [c]	0.08 ± 0.02	1994
P11	13314491	335996	0.17 ± 0.04	2005
Z1 [d]	3145322 (+ 3 Nm³ gas condensate)	n.a.	no enh.	1993
Z2 [d]	14321737 (+ 198 Nm³ gas condensate)	n.a.	no enh.	2003
Z3	0	n.a.	no enh.	1987
Z4	3794100	n.a.	no enh.	1985
Z5	0	n.a.	no enh.	2007
Z6	0	n.a.	no enh.	2004
Z7	13542079	n.a.	no enh.	2002
Z8	3251685	n.a.	no enh.	1990

[a] Zero gas production for the month of survey. Production only of delivering subsea wells.

[b] including one delivering subsea well

[c] gas production with little gas condensate (gas condensate is injected back into export gas)

[d] unmanned installation

525 Code and data availability

Access to the data is provided via request at the British Antarctic Survey Polar Data Centre.

Author contributions

The paper was written and figures were prepared by MP with contributions from AMGN. Modelling work was done by IP. All authors contributed to the discussion. The experimental design and flight planning were performed by GA, JL, TLC and DL. Aircraft set-up and in-flight measurements were performed by PB, PD, SA, SY, AW, TLC and JF. Laboratory measurements were made by REF, and data processing and calibrations were performed by JF, LH, PB, JS, PD.

Competing interests

The authors declare that they have no conflict of interest.

Acknowledgements

This work was funded under the Climate & Clean Air Coalition (CCAC) Oil and Gas Methane Science Studies (MSS) programme, hosted by the United Nations Environment Programme. Funding was provided by the Environmental Defense Fund (EDF), Oil and Gas Climate Initiative, European Commission, and CCAC.

Financial Support

This research has been supported by the Climate & Clean Air Coalition (CCAC) (grant no. DTIE18-EN018).

References

Brown, P., Cardenas, L., Del Vento, S., Karagianni, E., MacCarthy, J., Mullen, P., Passant, N., Richmond, B., Thistlethwaite, G., Thomson, A., Wakeling, D., Willis, D.: UK Greenhouse Gas Inventory 1990 to 2021: Annual Report for submission under the Framework Convention on Climate Change, Ricardo Energy & Environment for the Department for Business, Energy & Industrial Strategy (BEIS), Issue 1, ISBN: 978-0-9933975-9-2, 2023

Cain, M., Warwick N. J., Fisher, R. E., Lowry, D., Lanoisellé, M., Nisbet, E. G., France, J., Pitt, J., O'Shea, S., Bower, K. N., Allen, G., Illingworth, S., Manning, A. J., Bauguitte, S., Pisso, I., Pyle, J. A.: A study of a methane enhancement over the North Sea, J. Geophys. Res.-Atmos., 122, 7630-7645, https://doi.org/10.2002/2017JD026626, 2017

Chen, Z., Yacovitch, T. I., Daube, C., Herndon, S. C., Wilson, D., Enoch, S., Allen, D. T.: Reconciling methane emission measurements for offshore oil and gas platforms with detailed emission inventories: Accounting for emission intermittency, ChemRxiv. Cambridge: Cambridge Open Engage, Preprint, https://doi.org/10.26434/chemrxiv-2022-dfjvv, 2022

European Commission, United States of America: Global Methane Pledge, Climate & Clean Air Coalition (CCAC), https://www.ccacoalition.org/en/resources/global-methane-pledge (last access 30 November 2022), 2021

Conley, S., Franco, G., Faloona, I., Blake, D. R., Peischl, J., Ryerson, T. B.: Methane emissions from the 2015 Aliso Canyon blowout in Los Angeles, CA. Science, 351(6279), 1317-1320, https://www.science.org/doi/abs/10.1126/science.aaf2348, 2016

555 OPRED (BEIS): EEMS Atmospheric Emissions Calculations, Issue 1.810a, https://assets.publishing.service.gov.uk/government/uploads/system/uploads/attachment_data/file/136461/atmos-calcs.pdf (last access: 30 November 2022), 2008

Elvidge, C. D., Zhizhin, M., Hsu, F.-C., Baugh, K. E.: VIIRS Nightfire: Satellite Pyrometry at Night, Remote Sens., 5(9), 4423-4449, https://doi.org/10.3390/rs5094423, 2013

560 Elvidge, C. D., Zhizhin, M., Baugh, K., Hsu, F.-C., Ghosh, T.: Methods for Global Survey of Natural Gas Flaring from Visible Infrared Imaging Radiometer Suite Data, Energies 9(1), 14, https://doi.org/10.3390/en9010014, 2015

European Commission: EU strategy to reduce methane emissions, https://energy.ec.europa.eu/documents_en?f%5B0%5D=document_title%3AEU%20methane%20strategy (last access: 30 November 2022), 2020

565 Eurostat (European Commission): Energy, transport and environment statistics – 2020 edition: Energy Production 2018 (p. 11), Publications Office of the European Union, https://doi.org/10.2785/522192, 2020

Foulds, A., Allen, G., Shaw, J. T., Bateson, P., Barker, P. A., Huang, L., Pitt, J. R., Lee, J. D., Wilde, S. E., Dominutti, P., Purvis, R. M., Lowry, D., France, J. L. Fisher, R. E., Fiehn, A., Pühl, M., Bauguitte, S. J. B., Conley, S. A., Smith, M. L., Lachlan-Cope, T., Pisso, J., Schwietzke, S.: Quantification and assessment of methane emissions from offshore oil and gas

570 facilities on the Norwegian continental shelf, Atmos. Chem. Phys., 22, 4303-4322, https://doi.org/10.5194/acp-22-4303-2022, 2022

France, J. L., Bateson, P., Dominutti, P., Allen, G., Andrews, S., Bauguitte, S., Coleman, M., Lachlan-Cope, T., Fisher, R. E., Huang, L., Jones, A. E., Lee, J., Lowry, D., Pitt, J., Purvis, R., Pyle, J., Shaw, J., Warwick, N., Weiss, A., Wilde, S., Witherstone, J., Young, S.: Facility level measurement of offshore oil and gas installations from a medium-sized airborne

575 platform: method development for quantification and source identification of methane emissions. Atmos. Meas. Tech., 14, 71-88, https://doi.org/10.5194/amt-14-71-2021, 2021

Forster, P., Storelvmo, T., Armour, K., Collins, W., Dufresne, J.-L., Frame, D., Lunt, D.J., Mauritsen, T., Palmer, M. D., Watanabe, M., Wild, M., Zhang, H.: The Earth's Energy Budget, Climate Feedbacks, and Climate Sensitivity. In Climate
580   Change 2021: The Physical Science Basis. Contribution of Working Group I to the Sixth Assessment Report of the Intergovernmental Panel on Climate Change [Masson-Delmotte, V., Zhai, P., Pirani, A., Connors, S. L., Péan, C., Berger, S., Caud, N., Chen, Y., Goldfarb, L., Gomis, M.I., Huang, M., Leitzell, K., Lonnoy, E., Matthews, J.B.R., Maycock, T.K., Waterfield, T., Yelekçi, O., Yu, R., Zhou, B. (eds.)]. Cambridge University Press, Cambridge, United Kingdom and New York, NY, USA, pp. 923–1054, https://doi.org/10.1017/9781009157896.009, 2021

585   Garman, K. E., Hill, K. A., Wyss, P., Carlsen, M., Zimmerman, J.R., Stirm, B. H., Carney, T. Q., Santini, R., Shepson, P. B.: An Airborne and Wind Tunnel Evaluation of a Wind Turbulence Measurement System for Aircraft-Based Flux Measurements. J. Atmos. Ocean. Technol., 23, 1696–1708, https://doi.org/10.1175/JTECH1940.1, 2006

Gorchov Negron, A. M., Kort, E. A., Conley, S. A., Smith, M. L.: Airborne Assessment of Methane Emissions from Offshore Platforms in the U.S. Gulf of Mexico. Environ. Sci. Technol., 54, 5112−5120, https://doi.org/10.1021/acs.est.0c00179, 2020

590   Hausmann, P., Sussmann, R., Smale, D.: Contribution of oil and natural gas production to renewed increase in atmospheric methane (2007-2014): top-down estimate from ethane and methane column observations. Atmos. Chem. Phys., 16, 3227–3244, https://doi.org/10.5194/acp-16-3227-2016, 2016

Hensen, A., Velzeboer, I., Frumau, K. F. A., van den Bulk, W. C. M., van Dinther, D.: Methane emission measurements of offshore oil and gas platforms, TNO Report 2019 R1089, National Institute for Public Health and the Environment, RIVM,
595   http://resolver.tudelft.nl/uuid:a9c705b9-ec88-4316-827f-f9d7ffbd05c2 (last access 30 November 2022), 2019

Honig, E., Montfoort, J. A., Dröge, R., Guis, B., Baas, K., van Huet, B., van Hunnik, O. R.: Methodology report on the calculation of emissions to air from the sectors Energy, Industry and Waste, RIVM report 2022-0001, National Institute for Public Health and the Environment, https://doi.org/10.21945/RIVM-2022-0001 (last access: 30 November 2022), 2022

Jones, V. T., Matthews, M. D., Richers, D. M.: Light hydrocarbons for petroleum and gas prospecting, Geochemical Remote
600   Sensing of the Subsurface, Handbook of Exploration Geochemistry, 7, 133-212, Elsevier, New York, https://doi.org/10.1016/S0168-6275(00)80029-X, 2000

Klausner, T., Mertens, M., Huntrieser, H., Galkowski, M., Kuhlmann, G., Baumann, R., Fiehn, A., Jöckel, P., Pühl, M., Roiger, A.: Urban greenhouse gas emissions from the Berlin area: A case study using airborne CO_2 and CH_4 in situ observations in summer 2018, Elem Sci Anth, 8: 15, https://doi.org/10.1525/elementa.411, 2020

605   Lan, X., Thoning, K. W., Dlugokencky, E. J.: Trends in globally-averaged CH4, N2O, and SF6 determined from NOAA Global Monitoring Laboratory measurements, Version 2022-11, https://doi.org/10.15138/P8XG-AA10, 2022

Lee, J. D., Mobbs, S. D., Wellpott, A., Allen, G., Bauguitte, S. J.-B., Burton, R. R., Camilli, R., Coe, H., Fisher, R. E., France, J. L., Gallagher, M., Hopkins, J. R., Lanoiselle, M., Lewis, A. C., Lowry, D., Nisbet, E. G., Purvis, R. M., O'Shea, S., Pyle, J. A., Ryerson, T. B.: Flow rate and source reservoir identification from airborne chemical sampling of the uncontrolled Elgin

610   platform gas release, Atmos. Meas. Tech., 11, 1725–1739, https://doi.org/10.5194/amt-11-1725-2018, 2018

Lowry, D., Fisher, R. E., France, J. L., Coleman, M., Lanoisellé, M., Zazzeri, G., Nisbet, E. G., Shaw, J. T., Allen, G., Pitt, J., Ward, R. S.: Environmental baseline monitoring for shale gas development in the UK: Identification and geochemical characterisation of local source emissions of methane to atmosphere, Sci Total Environ, 708:134600, https://doi.org/10.1016/j.scitotenv.2019.134600, 2020

615   Lyon, D. R., Zavala-Araiza, D., Alvarez, R. A., Harris, R., Palacios, V., Lan, X., Talbot, R., Lavoie, T., Shepson, P., Yacovitch, T. I., Herndon, S. C., Marchese, A. J., Zimmerle, D., Robinson, A. L., Hamburg, S. P.: Constructing a Spatially Resolved Methane Emission Inventory for the Barnett Shale Region, Environ. Sci. Technol., 49, 13, 8147–8157, https://doi.org/10.1021/es506359c, 2015

MacKay, K., Lavoie, M., Bourlon, E., Atherton, E., O'Connell, E., Baillie, J., Fougère, C., Risk, D.: Methane emissions from

620   upstream oil and gas production in Canada are underestimated, Sci Rep 11, 8041, https://doi.org/10.1038/s41598-021-87610-3, 2021

Nara, H., Tanimoto, H., Tohjima, Y., Mukai, H., Nojiri, Y., Machida, T.: Emissions of methane from offshore oil and gas platforms in Southeast Asia, Sci Rep 4, 6503, https://doi.org/10.1038/srep06503, 2014

Nisbet, E. G., Manning, M. R., Dlugokencky, E. J., Fisher, R. E., Lowry, D., Michel, S. E., Lund Myhre, C., Platt, S. M., Allen,

625   G., Bousquet, P., Brownlow, R., Cain, M., France, J. L., Hermansen, O., Hossaini, R., Jones, A. E., Levin, I., Manning, A. C., Myhre, G., Pyle, J. A., Vaughn, B. H., Warwick, N. J., White, J. W. C.: Very strong atmospheric methane growth in the 4 years 2014–2017: Implications for the Paris Agreement. Global Biogeochemical Cycles, 33, 318-342, https://doi.org/10.1029/2018GB006009, 2019

Oil and Gas Authority, OGA: UKCS Flaring and Venting Report. https://ogauthorityreports.wixsite.com/ukcs-f-v-report-2020

630   (last access: 30 November 2022), 2020

O'Shea, S. J., Allen, G., Gallagher, M. W., Bower, K., Illingworth, S. M., Muller, J. B. A., Jones, B. T., Percival, C. J., Bauguitte, S. J-B., Cain, M., Warwick, N., Quiquet, A., Skiba, U., Drewer, J., Dinsmore, K., Nisbet, E. G., Lowry, D., Fisher,

R. E., France, J. L., Aurela, M., Lohile, A., Hayman, G., George, C., Clark, D. B., Manning, A. J., Friend, A. D., Pyle, J.: Methane and carbon dioxide fluxes and their regional scalability for the European Arctic wetlands during the MAMM project in summer 2012. Atmos. Chem. Phys., 14, 13159–13174. https://doi.org/10.5194/acp-14-13159-2014, 2014

Pandey, S., Gautam, R., Houweling, S., van der Gon, H. D., Sadavarte, P., Borsdorff, T., Hasekamp, O., Landgraf, J., van Kempen, T., Hoogeveen, R., van Hees, R., Hamburg, S. P., Maasakkers, J. D., Aben, I.: Satellite observations reveal extreme methane leakage from a natural gas well blowout, Proceedings of the National Academy of Sciences, 116 (52) 26376-26381, https://doi.org/10.1073/pnas.1908712116, 2019

Peischl, J., Eilerman, S. J., Neuman, J. A., Aikin, K. C., de Gouw, J., Gilman, J. B., Herndon, S. C., Nadkarni, R., Trainer, M., Warneke, C., Ryerson, T., B.: Quantifying methane and ethane emissions to the atmosphere from central and western U.S. oil and natural gas production regions. Journal of Geophysical Research: Atmospheres, 123, 7725– 7740, https://doi.org/10.1029/2018JD028622, 2018

Pétron, G., Karion, A., Sweeney, C., Miller, B. R., Montzka, S. A., Frost, G. J., Trainer, M., Tans, P., Andrews, A., Kofler, J., Helmig, D., Guenther, C., Dlugokencky, E., Lang, P., Newberger, T., Wolter, S., Hall, B., Novelli, P., Brewer, A., Conley, S., Hardesty, M., Banta, R., White, A., Noone, D., Wolfe, D., Schnell, R.: A new look at methane and nonmethane hydrocarbon emissions from oil and natural gas operations in the Colorado Denver-Julesburg Basin, J. Geophys. Res. Atmos., 119, 6836-6852, https://doi.org/10.1002/2013JD021272, 2014

Pisso, I., Sollum, E., Grythe, H., Kristiansen, N. I., Cassiani, M., Eckhardt, S., Arnold, D., Morton, D., Thompson, R. L., Groot Zwaaftink, C. D., Evangeliou, N., Sodemann, H., Haimberger, L., Henne, S., Brunner, D., Burkhart, J. F., Fouilloux, A., Brioude, J., Philipp, A., Seibert, P., Stohl, A.: The Lagrangian particle dispersion model FLEXPART version 10.4. Geosci. Model Dev., 12, 4955-4997, https://doi.org/10.5194/gmd-12-4955-2019, 2019

Pitt, J. R., Allen, G., Bauguitte, S. J.-B., Gallagher, M. W., Lee, J. D., Drysdale, W., Nelson, B., Manning, A. J., Palmer, P. I.: Assessing London CO2, CH4 and CO emissions using aircraft measurements and dispersion modelling. Atmos. Chem. Phys., 19, 8931–8945, https://doi.org/10.5194/acp-19-8931-2019, 2019

Riddick, S. N., Mauzerall, D. L., Celia, M., Harris, N. R. P., Allen, G., Pitt, J., Staunton-Sykes, J., Forster, G. L., Kang, M., Lowry, D., Nisbet, E. G., Manning, A. J.: Methane emissions from oil and gas platforms in the North Sea, Atmos. Chem. Phys., 19, 9787–9796, https://doi.org/10.5194/acp-19-9787-2019, 2019

Roiger, A., Thomas, J.-L., Schlager, H., Law, K. S., Kim, J., Schäfler, A., Winzierl, B., Dahlkötter, F., Krisch, I., Marelle, L., Minikin, A., Raut, J.-C., Reiter, A., Rose, M., Scheibe, M., Stock, P., Baumann, R., Bouarar, I., Clerbaux, C. George, M.,

Onishi, T., Flemming, J.: Quantifying Emerging Local Anthropogenic Emissions in the Arctic Region: The ACCESS Aircraft Campaign Experiment. Bull. Amer. Meteor. Soc., 96(3), 441-460, https://doi.org/10.1175/BAMS-D-13-00169.1., 2015

665 Saunois, M., Stavert, A. R., Poulter, B., Bousquet, P., Canadell, J. G., Jackson, R. B., Raymond, P. A., Dlugokencky, E. J., Houweling, S., Patra, P. K., Ciais, P., Arora, V. K., Bastviken, D., Bergamaschi, P., Blake, D. R., Brailsford, G., Bruhwiler, L., Carlson, K. M., Carrol, M. Castaldi, S., Chandra, N., Crevoisier, C., Crill, P. M., Covey, K., Curry, C. L., Etiope, G., Frankenberg, C., Gedney, N., Hegglin, M. I., Höglund-Isaksson, L., Hugelius, G., Ishizawa, M., Ito, A., Janssens-Maenhout, G., Jensen, K., Joos, F., Kleinen, T., Krummel, P. B., Langenfels, R. L., Laruelle, G. G., Liu, L., Machida, T., Maksyutov, S., McDonald, K. C., McNorton, J., Miller, P. A., Melton, J. R., Morino, I., Müller, J., Murguia-Flores, F., Naik, V., Niwa, Y., Noce, S., O'Doherty, S., Parker, R. J., Peng, C. Peng, S., Peters, G. P., Prigent, C., Prinn, R., Ramonet, M., Regnier, P., Riley,
670 W. J., Rosentreter, J. A., Segers, A., Simpson, I. J., Shi, H., Smith, S. J., Steele, L. P., Thornton, B. F., Tian, H., Tohjima, Y., Tubiello, F. N., Tsuruta, A., Viovy, N., Voulgarakis, A., Weber, T. S., van Weele, M., van der Werf, G. R., Weiss, R. F., Worthy, D., Wunch, D. Yin, Y., Yoshida, Y., Zhang, W., Zhang, Z., Zhao, Y., Zheng, B., Zhu, Q., Zhu, Q., Zhuang, Q.: The Global Methane Budget 2000–2017, Earth Syst. Sci. Data, 12, 1561–1623, https://doi.org/10.5194/essd-12-1561-2020, 2020

Scarpelli, T. R., Jacob, D. J.: Global Fuel Exploitation Inventory (GFEI). Harvard Dataverse, V2,
675 https://doi.org/10.7910/DVN/HH4EUM., 2019

Scarpelli, T. R., Jacob, D. J., Maasakkers, J. D., Sulprizio, M. P., Sheng, J.-X., Rose, K., Romeo, L., Worden, J. R., Janssens-Maenhout, G.: A global gridded (0.1° × 0.1°) inventory of methane emissions from oil, gas, and coal exploitation based on national reports to the United Nations Framework Convention on Climate Change. Earth Syst. Sci. Data, 12, 563–575, https://doi.org/10.5194/essd-12-563-2020, 2020

680 Schwietzke, S., Sherwood, O., Bruhwiler, L. M. P., Miller, J. B., Etiope, G., Dlugokencky, E. J., Englund Michel, S., Arling, V., A., Vaughn, B. H., White, J. W. C., Tans, P. P.: Upward revision of global fossil fuel methane emissions based on isotope database, Nature 538, 88–91, https://doi.org/10.1038/nature19797, 2016

Smith, M. L., Kort, E. A., Karion, A., Sweeney, C., Herndon, S. C., Yacovitch, T. I.: Airborne Ethane Observations in the Barnett Shale: Quantification of Ethane Flux and Attribution of Methane Emissions. Environ. Sci. Technol., 59 (13), 8158-
685 8166, https://pubs.acs.org/doi/abs/10.1021/acs.est.5b00219, 2015

Stull, R. B. (1988): An Introduction to Boundary Layer Meteorology, Atmospheric Sciences Library, Springer, Dordrecht, https://doi.org/10.1007/978-94-009-3027-8, 2015

Tullos, E. E., Stokes, S. N., Cardoso-Saldaña, F., J., Herndon, S. C., Smith, B. J., Allen, D. T.: Use of Short Duration Measurements to Estimate Methane Emissions at Oil and Gas Production Sites. Environ. Sci. Technol. Lett. 8 (6). 463-467,
690   https://doi.org/10.1021/acs.estlett.1c00239, 2021

UNFCCC: Greenhouse Gas Inventory Data Interface, http://di.unfccc.int/detailed_data_by_party (last access: 14 March 2022), 2022

Varon, D. J., McKeever, J., Jervis, D., Maasakkers, J. D., Pandey, S., Houweling, S.: Satellite discovery of anomalously large methane poin sources from oil/gas production. Geophysical Research Letters, 46, 13507-13516,
695   https://doi.org/10.1029/2019GL083798, 2019

Weiss, A. I., King, J., Lachlan-Cope, T., Ladkin, R.: On the effective aerodynamic and scalar roughness length of Weddell Sea ice. J. Geophys. Res.-Atmos., 116, D19119, https://doi.org/10.1029/2011JD015949, 2011

Whiticar, M. J.: Correlation of natural gases with their sources. In The petroleum system-from source to trap. Magoon, L. B., Dow, W.G., Eds., AAPG, pp 261-283, 1994

700   Xiao, Y., Logan, J. A., Jacob, D. J., Hudman, R. C., Yantosca, R., Blake, D. R.: Global budget of ethane and regional constraints on US sources, J. Geophys. Res, 113(D21): 306, https://doi.org/10.1029/2007JD009415, 2008

Yacovitch, Tara I., Herndon, S. C., Roscioli, J. R., Floerchinger, C., McGovern, R. M., Agnese, M., Pétron, G., Kofler, J., Sweeney, C., Karion, A., Conley, S. A., Kort, E. A., Nähle, L., Fischer, M. Hildebrandt, L., Koeth, J., McMaunus, J. B., Nelson, D. D., Zahniser, M. S., Kolb, C. E.: Demonstration of an Ethane Spectrometer for Methane Source Identification,
705   Environ. Sci. Technol. 48, 14, 8028–8034, https://doi.org/10.1021/es501475q, 2014

Yacovitch, T. I., Daube, C., Herndon, S. C.: Methane Emissions from Offshore Oil and Gas Platforms in the Gulf of Mexico, Environ. Sci. Technol. 54, 6, 3530–3538, https://doi.org/10.1021/acs.est.9b07148, 2020

Zavala-Araiza, D., Alvarez, R. A., Lyon, D. R., Allen, D. T., Marchese, A. J., Zimmerle, D. J., Hamburg, S. P.: Super-emitters in natural gas infrastructure are caused by abnormal process conditions. Nat Commun 8, 14012,
710   https://doi.org/10.1038/ncomms14012, 2017

Zavala-Araiza, D., Omara, M., Gautam, R., Smith, M. L., Pandey, S., Aben, I., Almanza-Veloz, V., Conley, S., Houweling, S., Kort, E.A.: A tale of two regions: methane emissions from oil and gas production in offshore/onshore Mexico, Environ. Res. Lett., 16(2), https://doi.org/10.1088/1748-9326/abceeb, 2021